Results of an all-sky high-frequency Einstein@Home search for continuous gravitational waves in LIGO 5th Science Run

Avneet Singh[1,2,3,a], Maria Alessandra Papa[1,2,4], Heinz-Bernd Eggenstein[2,3], Sylvia Zhu[1,2], Holger Pletsch[2,3], Bruce Allen[2,4,3], Oliver Bock[2,3], Bernd Maschenchalk[2,3], Reinhard Prix[2,3], Xavier Siemens[4]

[1] *Max-Planck-Institut für Gravitationsphysik, am Mühlenberg 1, 14476, Potsdam-Golm*
[2] *Max-Planck-Institut für Gravitationsphysik, Callinstraße 38, 30167, Hannover*
[3] *Leibniz Universität Hannover, Welfengarten 1, 30167, Hannover*
[4] *University of Wisconsin-Milwaukee, Milwaukee, Wisconsin 53201, USA*

(Dated: June 22, 2016)

We present results of a high-frequency all-sky search for continuous gravitational waves from isolated neutron stars in LIGO 5th Science Run (S5) data, using the computing power of the Einstein@Home volunteer computing project. This is the only dedicated continuous gravitational wave search that probes this high frequency range on S5 data. We find no significant candidate signal, so we set 90%-confidence level upper-limits on continuous gravitational wave strain amplitudes. At the lower end of the search frequency range, around 1250 Hz, the most constraining 90%-confidence upper-limit is 4.96×10^{-24}, while at the higher end, around 1500 Hz, it is 6.0×10^{-24}. Based on these upper-limits, and assuming fiducial value of the principal moment of inertia of $10^{38}\,\mathrm{kg\,m^2}$, we can exclude objects with ellipticities higher than roughly 2.8×10^{-7} within 100 pc of Earth with rotation periods between 1.3 and 1.6 milliseconds.

I. INTRODUCTION

Ground-based gravitational wave (GW) detectors will be able to detect a continuous gravitational wave signal from a spinning deformed compact object provided that it is spinning with a rotational period between roughly 1 and 100 milliseconds, that it is sufficiently close to Earth and sufficiently "bumpy". Blind searches for continuous gravitational waves probe the whole sky and broad frequency ranges, looking for these type of objects.

In this paper, we present the results of an all-sky Einstein@Home search for continuous, nearly monochromatic gravitational waves in the high frequency range in data from LIGO's 5th Science Run (S5). A number of searches have been carried out on LIGO data [2, 4, 5, 7–9] targeting lower frequency ranges. The only other search covering frequencies up to 1500 Hz was conducted on S6 data [10]. The search reported here also covers the high frequency range but uses a different data set. It can be considered an extension of the S5 Einstein@Home search [2] although it employs a different search technique: this search uses the GCT method to combine results from coherent *F-statistic* searches [13, 14], as opposed to the previous Einstein@Home search [2] that employed the *Hough-transform* method to perform this combination. In the end, at fixed computing resources, these two search methods are comparable in sensitivity.

We do not find any significant signal(s) among the set of searched waveforms. Thus, we set 90%-confidence upper-limits on continuous gravitational wave strain amplitudes; near the lower end of the search frequency range between 1253.217–1255.217 Hz, the most constraining upper-limit is 4.96×10^{-24}, while toward the higher end of the search frequency range nearing 1500 Hz, the upper-limit value is roughly 6.0×10^{-24}. Consequently, based on these upper-limits, we can exclude certain combinations of signal frequency, star deformation (ellipticity) and distance values. We show with this search that even with S5 data from the first generation of GW detectors, such constraints do probe interesting regions of source parameter space.

II. THE DATA

The LIGO gravitational wave network consists of two detectors, H1 in Hanford (Washington) and L1 in Livingston (Louisiana), separated by a 3000-km baseline. The S5 run lasted roughly two years between the GPS time 815155213 sec (Fri, Nov 04, 16:00:00 UTC 2005) and 875145614 sec (Sun, Sep 30, 00:00:00 UTC 2007). This search uses data spanning this observation period, and during this time, H1 and L1 had duty-factors of 78% and 66% respectively [3, 6]. The gaps in this data-set are due to environmental or instrumental disturbances, or scheduled maintenance periods.

We follow [2, 4], where the calibrated and high-pass filtered data from each detector is partitioned in 30-minute chunks and each chunk is Fourier-transformed after the application of a steep Tukey window. The set of **S**hort (time-baseline) **F**ourier transforms (SFT) that ensues, is the input data for our search.

[a] email: avneet.singh@aei.mpg.de

We further follow [2], where frequency bands known to contain spectral disturbances have been removed from the analysis. In fact, such data has been substituted with fake Gaussian noise at the same level as the neighboring undisturbed data; in Table III, we list these bands.

III. THE SEARCH

The search presented here is similar to the search on S6 data, reported in [9]. Our reference target signal is given, for example, by (1)-(4) in [7]; at emission, the signal is nearly monochromatic, typically with a small "spindown". The signal waveform in the detector data is modulated in frequency because of the relative motion between the compact object and the detector; a modulation in amplitude also occurs because of the variation of the sensitivity of the detector with time across the sky.

The most sensitive search technique that one could use is a fully-coherent combination of the detectors' data, matched to the waveform that one is looking for. The (amplitude) sensitivity of such a method increases with the square-root of the time-span of the data used. However the computational cost to resolve different waveforms increases very rapidly with increasing time-span of the data, and this makes a fully-coherent search over a large frequency range using months of data, computationally unfeasible. This is the main reason why semi-coherent search methods have been developed. These methods perform coherent searches over shorter stretches of data, called segments, and then combine the results with incoherent techniques.

This search covers waveforms from the entire sky, with frequencies in a 250 Hz range from 1249.717 Hz to 1499.717 Hz, and with a first-order spin-down between -2.93×10^{-9} Hz/s and 5.53×10^{-10} Hz/s. We use a stack–slide semi-coherent search procedure implemented with the GCT method [13, 14]. The data is divided into $N_{\rm seg}$ segments each spanning $\mathrm{T_{coh}}$ in time. The coherent multi-detector $\mathcal{F}$-statistic [11] is computed on each segment for all the points on a coarse $\lambda_{\rm c} \equiv (f_{\rm c}, \dot{f}_{\rm c}, \alpha_{\rm c}, \delta_{\rm c})$ signal waveform parameter grid, and then results from the individual segments are summed, one per segment, to yield the final core detection-statistic $\overline{\mathcal{F}}$, as shown in (1); α, δ are the equatorial sky coordinates of the source position, while f and $\dot{f}$ are the frequency and first-order spin-down of the signal respectively. Depending on what $\lambda_{\rm c}$ parameter points are taken on the coarse grid for each segment in this sum, the result will approximate the detection-statistic computed on a λ_f parameter point on a finer grid.

$$\overline{\mathcal{F}}(\lambda_f) := \frac{1}{N_{\rm seg}} \sum_{i=1}^{N_{\rm seg}} \mathcal{F}(\lambda_{\rm c}^i) \qquad (1)$$

In a stack–slide search in Gaussian noise, $N_{\rm seg} \times 2\overline{\mathcal{F}}$ follows a $\chi^2_{4N_{\rm seg}}$ chi-squared distribution with $4N_{\rm seg}$ degrees of freedom.

The most important search parameters are then: $N_{\rm seg}$, $\mathrm{T_{coh}}$, the signal parameter search grids $\lambda_{\rm c}$, λ_f, the total spanned observation time $\mathrm{T_{obs}}$, and finally the ranking statistic used to rank parameter space cells i.e. $2\overline{\mathcal{F}}$.

The grid-spacing in frequency δf and spin-down $\delta \dot{f}$ are constant over the search range. The same frequency spacing and sky grid is used for coherent analysis and in the incoherent summing. The spin-down spacing of the incoherent analysis is finer by a factor of γ with respect to that of the coherent analysis. In Table I, we summarize the search parameters.

The sky-grid for the search is constructed by tiling the projected equatorial plane uniformly with squares of edge length $d_{\rm sky}$. The length of the edge of the squares is a function of frequency of the signal f, and parameterized in terms of a so-called *sky-mismatch parameter* ($\mathrm{m_{sky}}$) as follows

$$d_{\rm sky} = \frac{1}{f} \frac{\sqrt{\mathrm{m_{sky}}}}{\pi \tau_{\rm E}} \qquad (2)$$

where, $\tau_{\rm E} = 0.021$ seconds and $\mathrm{m_{sky}} = 0.3$, also given in Table I. The sky-grids are constant over 10 Hz-wide frequency bands, and are calculated for the highest frequency in the band. In Fig.1, we illustrate the sky-grid for the 1240-1250 Hz band. The total number of templates in 50 mHz bands as a function of frequency is shown in Fig.2. This search explores a total of 5.6×10^{16} waveform templates across the $\lambda_f \equiv (f_f, \dot{f}_f, \alpha_f, \delta_f)$ parameter space.

The search is divided into smaller work-units (WU) and each WU searches a very small sub-set of template waveforms. The WUs are sent to Einstein@Home volunteers and each WU occupies the volunteer/host computer for roughly 6 hours. One such WU covers a 50-mHz band, the entire spin-down range, and 139–140 points in the sky. 6.4 million different WUs are necessary to cover the whole parameter space. Each WU returns a ranked list of the most significant 10^4 points in the parameter space that it searched.

IV. IDENTIFICATION OF UNDISTURBED BANDS

In Table III, we list the central frequencies and bandwidths of SFT data known to contain spectral lines from instrumental artefacts. These frequency regions were identified before the Einstein@Home run, and we were able to replace the corresponding data with Gaussian noise matching the noise level of neighbouring quiet bands. Consequently, some search results have contributions from this 'fake data'. The intervals in signal-frequency where the search results come entirely from fake data are indicated as *all fake data* in Table IV. In these intervals of signal-frequency, we effectively do not have search results. The other 3 columns in Table IV provide signal-frequency intervals where results *might* have contributions from fake data.

as "disturbed", and rankings of '1' or '2' mark the band as "marginally disturbed". A 50-mHz band is eventually considered to be undisturbed if it is marked as '0' by both scientists. The criteria used for this inspection are based on training-sets of real data containing simulated signals. These criteria are designed to exclude disturbed set of results while retaining data sets with signal-like properties, and to err on the side of being conservative in terms of not falsely dismissing signal-like distributions of $2\overline{\mathcal{F}}$ values. In Fig.3, we empirically illustrate these criteria using three examples. In this search, 3% of the total 5000 50-mHz bands are marked as "disturbed" by visual inspection. These excluded bands are listed in Table V (Type D), together with the 50-mHz bands excluded as a result of the cleaning of known disturbances above, i.e. marked as "all fake data" (Type C).

In Fig.4, we plot the loudest observed candidate i.e. the candidate with the highest $2\overline{\mathcal{F}}$ value in each 0.5 Hz band of the search frequency range. The loudest candidate in our search has a detection-statistic value of $2\overline{\mathcal{F}} = 5.846$ at a frequency of roughly 1391.667 Hz. In order to determine the significance of this loudest candidate, we compare it to the expected value for the highest detection-statistic in our search. In order to determine this expected value, we have to estimate the number of independent trials performed in the search i.e. total number of independent realizations of our detection-statistic $2\overline{\mathcal{F}}$. Finally, the loudest expected value of $2\overline{\mathcal{F}}$ is the average of $N_{\rm seg} = 205$ χ^2 variables with 4 degrees of freedom over $N_{\rm trials}$ independent trials, and it can be determined by integration of the probability density function given, for example, by (5)-(6) of [1].

The number of independent realizations of the detection-statistic, $N_{\rm trials}$, in a search through a bank of signal templates is smaller than the total number of searched templates, $N_{\rm templates}$. We estimate $N_{\rm trials}$ as a function of frequency in 10 Hz frequency intervals. In each of these 10 Hz intervals, we fit the distribution of loudest candidates from 50 mHz bands contained within the 10 Hz interval to the expected distribution [1], and obtain the best-fitted value of $N_{\rm trials}$. We perform this calculation in 10 Hz intervals since the sky-grids, along with $N_{\rm templates}$, are constant over 10 Hz frequency intervals.

In Fig.5, we plot the ratio $\mathcal{R} = N_{\rm trials}/N_{\rm templates}$, as a function of frequency. We observe that $\mathcal{R}$ decreases with frequency, suggesting that the net increase in finesse of the grid with respect to frequency in higher than the actual increase in sky resolution. This effect is confirmed in Fig.6.

With $\mathcal{R}(f)$ in hand, we evaluate the expected value for the loudest detection-statistic ($2\overline{\mathcal{F}}_{\rm exp}$) in 0.5 Hz bands, and the standard deviation ($\sigma_{\rm exp}$) of the associated distribution using (5)-(6) of [1], with $N_{\rm seg} = 205$ and $N_{\rm trials} = \mathcal{R}\, N_{\rm templates}$. Based on these values, we can estimate the significance of our observed loudest candidates (denoted by $2\overline{\mathcal{F}}_{\rm Loud}$) as the Critical Ratio (CR),

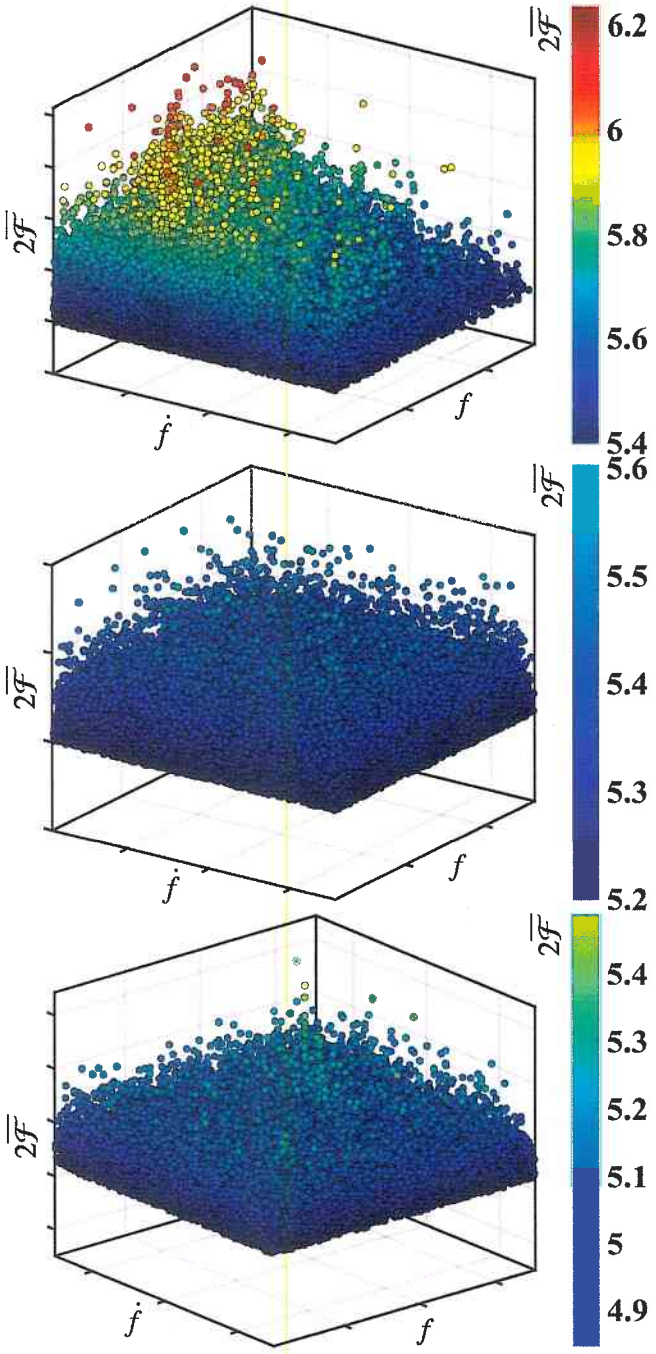

FIG. 3. We plot the color-coded $2\overline{\mathcal{F}}$ values on the z-axis in three 50 mHz bands. The top-most band is marked as "disturbed"; the middle band is an example of an "undisturbed" band; the bottom-most band is an example of an undisturbed band but containing a simulated continuous gravitational wave signal.

$$\mathrm{CR} := \frac{2\overline{\mathcal{F}}_{\rm Loud} - 2\overline{\mathcal{F}}_{\rm exp}}{\sigma_{\rm exp}}. \qquad (3)$$

In Fig.7, we plot the CR values of the observed loudest

with this null result at 90%-confidence in 0.5-Hz bands. Here, $h_0^{90\%}$ is the gravitational wave amplitude for which 90% of the target population of signals would have produced a value of the detection statistic higher than the observed value.

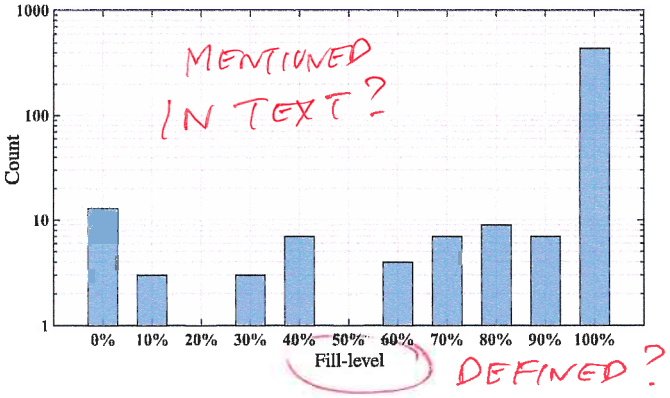

FIG. 8. Distribution of fill-levels of 0.5 Hz bands.

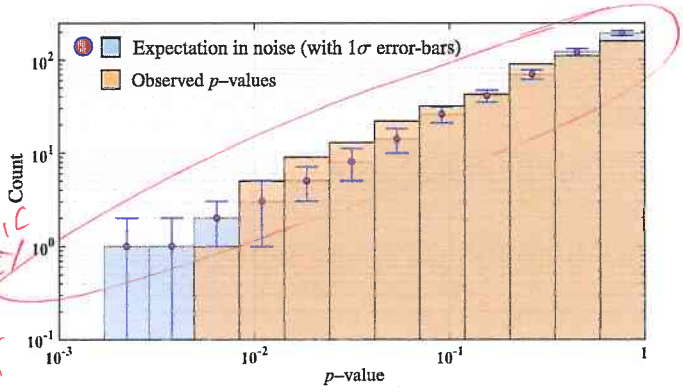

FIG. 9. p-values for the loudest observed candidates in 0.5 Hz bands in the data (top brown histogram bars), and the expected distribution of p-values for pure noise for reference (bottom blue histogram bars with markers).

Ideally, in order to estimate the $h_0^{90\%}$ values in each 0.5 Hz band across the 250-Hz signal-frequency search range, we would perform Monte-Carlo injection-and-recovery simulations in each of those bands. However, this is computationally very intensive and impractical. Therefore, we perform Monte-Carlo simulations in six 0.5-Hz bands spread evenly across the 250-Hz-wide frequency range, and in each of these six bands labeled by the index j, we estimate the $h_{0,\mathrm{CR}_i}^{90\%,k}$ upper-limit value corresponding to eight different CR_i significance bins for the putative observed loudest candidate: $(0.0, 0.5, 1.0, 1.5, 2.0, 2.5, 3.0, 3.5)$. In each of these six bands and for each of the eight detection criteria, we calculate the so-called 'sensitivity-depth', defined in [1]: $\mathcal{D}_{\mathrm{CR}_i}^{90\%,k}$. Lastly, we average these sensitivity-depths over the 6 bands and derive the average sensitivity-depth $\mathcal{D}_{\mathrm{CR}_i}^{90\%,k}$ for each detection criteria. The values of the sensitivity-depths range between $\mathcal{D}_{\mathrm{CR}_{0.0}}^{90\%} = 30.7\,\mathrm{Hz}^{-1/2}$ and $\mathcal{D}_{\mathrm{CR}_{3.5}}^{90\%} = 28.9\,\mathrm{Hz}^{-1/2}$. We use these $\mathcal{D}_{\mathrm{CR}_i}^{90\%}$ values to set upper-limits in the bands (again labeled by k) where we have not performed any Monte-Carlo simulations as follows:

$$h_0^{90\%}(f_k) = \frac{\sqrt{S_h(f_k)}}{\mathcal{D}_{\mathrm{CR}_{i(k)}}^{90\%}} \tag{4}$$

where, CR_i is the significance bin corresponding to the loudest observed candidate in the i-th frequency band, and $S_h(f_k)$ is the average amplitude spectral density of the data in that band, measured in $\mathrm{Hz}^{-1/2}$. The uncertainties on the $h_0^{90\%}$ upper-limit values introduced by this procedure amount to roughly 10% of the nominal $h_0^{90\%}$ upper-limit value. The final $h_0^{90\%}$ upper-limit values for this search, including an additional 10% calibration uncertainty, are given in Table II, and shown in Fig.10.

Note that we do not set upper limits in 0.5-Hz bands where the results are entirely produced with fake Gaussian data inserted by the cleaning procedure described in section IV; $h_0^{90\%}$ upper-limit values for such bands do not appear in either Table II, or in Fig.10. Moreover, there also exist 50-mHz bands that contain results contributed by entirely fake data as a result of the cleaning procedure, or that have been excluded from the analysis because they are marked as disturbed by the visual inspection method described in section IV. We mark the 0.5-Hz bands which host these particular 50-mHz bands with a different color (bright red markers) in Fig.10. In Table V, we provide a complete list of such 50-mHz bands highlighting that the upper-limit values do not apply to these listed 50 mHz bands. Finally, we note that, due to the cleaning procedure, there exist signal-frequency bands where the search results *may* have contributions from some fake data. We list these signal-frequency ranges in Table IV. In line with the remarks in section IV, and for the sake of completeness, Table IV also contains the cleaned bands that featured under Type C in Table V, under the column header "All Fake Data".

VI. CONCLUSIONS

This search did not yield any significant evidence of continuous gravitational waves in the LIGO 5th Science Run data in the high-frequency range of 1250–1500 Hz. The lowest value for the upper-limit is 4.96×10^{-24} for signal frequencies between 1253.217–1255.217 Hz. We show in Fig.10 that these $h_0^{90\%}$ upper-limits are about 33% larger than the upper-limits[1] set [10] in the same frequency range but using S6 data. In this frequency range,

[1] The upper-limit values of [10] have been re-scaled according to [17] in order to allow a direct comparison with our $h_0^{90\%}$ upper-limit results.

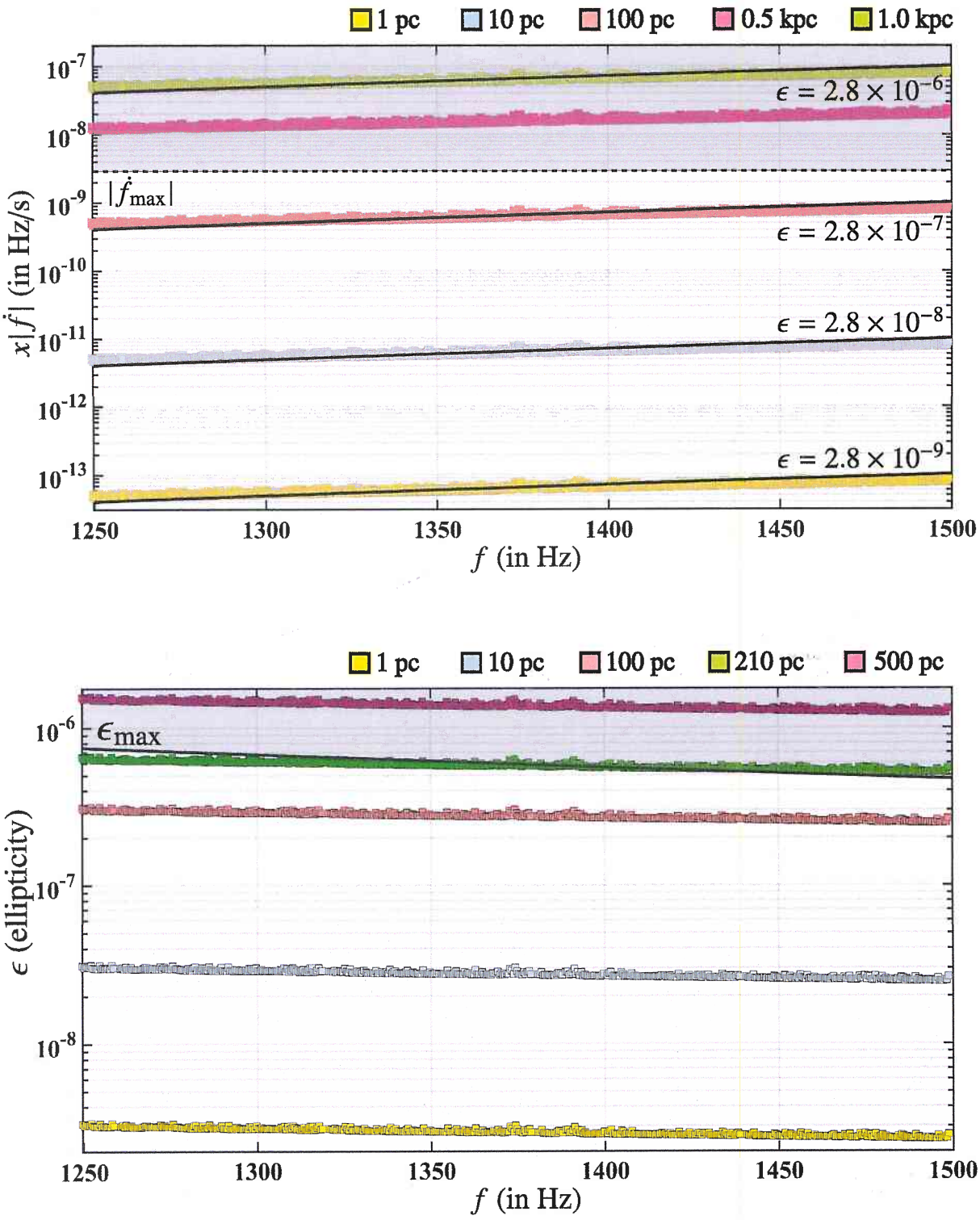

FIG. 11. Gravitational wave amplitude upper-limits recast as curves in the $(f, x|\dot{f}|)$-plane (top panel) for sources at given distances, where f is the signal-frequency and $x|\dot{f}|$ is the gravitational wave spin-down i.e. the fraction of the actual spin-down $|\dot{f}|$ that accounts for the rotational energy loss due to gravitational wave emission. We have superimposed the curves of constant ellipticity ϵ. The dotted line at $|\dot{f}_{\rm max}|$ indicates the maximum magnitude of searched spin-down, namely 2.93×10^{-9} Hz/s. The bottom panel shows the corresponding (f, ϵ) upper-limit curves for sources at various distances. The $\epsilon_{\rm max} = 41.3 \times f^{-5/2}$ curve is the ellipticity corresponding to the highest $|\dot{f}|$ searched.

f (in Hz)	$h_0^{90\%} \times 10^{24}$
1305.217	5.2 ± 0.9
1307.217	5.3 ± 1.0
1309.217	5.2 ± 0.9
1311.217	5.2 ± 1.0
1313.217	5.3 ± 1.0
1315.217	5.5 ± 1.1
1317.217	5.3 ± 1.0
1320.717	5.3 ± 0.9
1322.717	5.2 ± 0.9
1324.717	5.2 ± 1.0
1326.717	5.5 ± 1.1
1328.717	5.3 ± 1.0
1330.717	5.4 ± 1.0
1332.717	5.2 ± 0.9
1334.717	5.2 ± 0.9
1336.717	5.3 ± 1.0
1338.717	5.3 ± 0.9
1340.717	5.3 ± 1.0
1342.717	5.4 ± 1.0
1344.717	5.4 ± 1.0
1346.717	5.3 ± 0.9
1348.717	5.3 ± 0.9
1350.717	5.3 ± 0.9
1352.717	5.3 ± 0.9
1354.717	5.6 ± 1.1
1356.717	5.4 ± 1.0
1358.717	5.3 ± 0.9
1360.717	5.4 ± 1.0
1362.717	5.7 ± 1.2
1364.717	5.5 ± 1.1
1366.717	5.4 ± 0.9
1368.717	5.5 ± 1.0
1370.717	5.4 ± 0.9
1372.717	5.9 ± 1.1
1374.717	5.7 ± 1.0
1376.717	5.6 ± 1.1
1378.717	5.5 ± 0.9
1382.217	5.4 ± 0.9
1384.217	5.5 ± 1.0
1386.217	5.6 ± 1.0
1388.717	5.7 ± 1.1
1390.717	5.7 ± 1.0
1392.717	5.5 ± 1.0
1394.717	5.5 ± 0.9
1396.717	5.5 ± 0.9
1398.717	5.5 ± 0.9
1401.217	5.7 ± 1.1
1403.217	5.5 ± 1.0
1405.217	5.7 ± 1.1

f (in Hz)	$h_0^{90\%} \times 10^{24}$
1305.717	5.2 ± 0.9
1307.717	5.4 ± 1.0
1309.717	5.3 ± 1.0
1311.717	5.3 ± 1.0
1313.717	5.2 ± 0.9
1315.717	5.5 ± 1.1
1317.717	5.5 ± 1.1
1321.217	5.3 ± 0.9
1323.217	5.2 ± 0.9
1325.217	5.5 ± 1.0
1327.217	5.3 ± 1.0
1329.217	5.2 ± 0.9
1331.217	5.3 ± 1.0
1333.217	5.2 ± 0.9
1335.217	5.2 ± 0.9
1337.217	5.4 ± 1.0
1339.217	5.4 ± 1.0
1341.217	5.3 ± 0.9
1343.217	5.5 ± 1.1
1345.217	5.3 ± 1.0
1347.217	5.3 ± 0.9
1349.217	5.3 ± 1.0
1351.217	5.3 ± 1.0
1353.217	5.3 ± 0.9
1355.217	5.4 ± 1.0
1357.217	5.6 ± 1.1
1359.217	5.3 ± 0.9
1361.217	5.4 ± 1.0
1363.217	5.3 ± 0.9
1365.217	5.4 ± 0.9
1367.217	5.4 ± 0.9
1369.217	5.6 ± 1.1
1371.217	5.4 ± 0.9
1373.217	5.7 ± 1.1
1375.217	5.5 ± 0.9
1377.217	5.5 ± 0.9
1380.717	5.5 ± 1.0
1382.717	5.5 ± 1.0
1384.717	5.4 ± 0.9
1386.717	5.7 ± 1.1
1389.217	5.8 ± 1.1
1391.217	6.0 ± 1.1
1393.217	5.8 ± 1.1
1395.217	5.5 ± 0.9
1397.217	5.5 ± 1.0
1399.217	5.5 ± 1.0
1401.717	5.8 ± 1.1
1403.717	5.5 ± 1.0
1405.717	5.5 ± 1.0

f (in Hz)	$h_0^{90\%} \times 10^{24}$
1306.217	5.2 ± 0.9
1308.217	5.2 ± 0.9
1310.217	5.4 ± 1.1
1312.217	5.2 ± 0.9
1314.217	5.2 ± 0.9
1316.217	5.2 ± 0.9
1318.217	5.2 ± 0.9
1321.717	5.2 ± 0.9
1323.717	5.3 ± 1.0
1325.717	5.3 ± 1.0
1327.717	5.2 ± 0.9
1329.717	5.3 ± 1.0
1331.717	5.2 ± 0.9
1333.717	5.2 ± 0.9
1335.717	5.4 ± 1.0
1337.717	5.3 ± 0.9
1339.717	5.4 ± 1.1
1341.717	5.3 ± 0.9
1343.717	5.3 ± 0.9
1345.717	5.3 ± 0.9
1347.717	5.6 ± 1.1
1349.717	5.4 ± 1.0
1351.717	5.3 ± 1.0
1353.717	5.3 ± 0.9
1355.717	5.3 ± 0.9
1357.717	5.4 ± 1.0
1359.717	5.5 ± 1.1
1361.717	5.3 ± 0.9
1363.717	5.3 ± 0.9
1365.717	5.4 ± 0.9
1367.717	5.5 ± 1.0
1369.717	5.4 ± 0.9
1371.717	5.5 ± 1.0
1373.717	5.5 ± 0.9
1375.717	5.5 ± 1.0
1377.717	5.7 ± 1.1
1381.217	5.5 ± 1.0
1383.217	5.4 ± 0.9
1385.217	5.5 ± 1.0
1387.217	5.6 ± 1.0
1389.717	5.5 ± 1.0
1391.717	5.6 ± 1.0
1393.717	5.5 ± 0.9
1395.717	5.5 ± 0.9
1397.717	5.5 ± 1.0
1399.717	5.7 ± 1.1
1402.217	5.5 ± 1.0
1404.217	5.5 ± 1.0
1406.217	5.6 ± 1.0

f (in Hz)	$h_0^{90\%} \times 10^{24}$
1306.717	5.3 ± 1.0
1308.717	5.4 ± 1.0
1310.717	5.3 ± 1.0
1312.717	5.3 ± 1.0
1314.717	5.4 ± 1.0
1316.717	5.2 ± 0.9
1318.717	5.3 ± 0.9
1322.217	5.3 ± 1.0
1324.217	5.3 ± 1.0
1326.217	5.2 ± 0.9
1328.217	5.2 ± 0.9
1330.217	5.2 ± 0.9
1332.217	5.2 ± 0.9
1334.217	5.4 ± 1.1
1336.217	5.2 ± 0.9
1338.217	5.5 ± 1.1
1340.217	5.3 ± 0.9
1342.217	5.3 ± 0.9
1344.217	5.3 ± 0.9
1346.217	5.3 ± 1.0
1348.217	5.3 ± 0.9
1350.217	5.3 ± 0.9
1352.217	5.3 ± 0.9
1354.217	5.3 ± 0.9
1356.217	5.3 ± 0.9
1358.217	5.3 ± 0.9
1360.217	5.3 ± 0.9
1362.217	5.3 ± 0.9
1364.217	5.3 ± 0.9
1366.217	5.4 ± 1.0
1368.217	5.5 ± 1.0
1370.217	5.5 ± 1.0
1372.217	5.5 ± 1.0
1374.217	6.0 ± 1.2
1376.217	5.4 ± 0.9
1378.217	5.7 ± 1.0
1381.717	5.7 ± 1.1
1383.717	5.5 ± 1.0
1385.717	5.4 ± 0.9
1387.717	5.5 ± 0.9
1390.217	5.6 ± 1.0
1392.217	5.8 ± 1.1
1394.217	5.6 ± 1.0
1396.217	5.5 ± 0.9
1398.217	5.5 ± 0.9
1400.717	5.5 ± 1.0
1402.717	5.5 ± 1.0
1404.717	5.8 ± 1.2
1406.717	5.6 ± 1.0

2. Detector Lines

Source	f (Hz)	Harmonics	LFS (Hz)	HFS (Hz)	IFO
Power Mains	60.0	5	1.0	1.0	L,H
Violin Mode	1373.75	1	0.1	0.1	H
Violin Mode	1374.44	1	0.1	0.1	H
Violin Mode	1377.14	1	0.1	0.1	H
Violin Mode	1378.75	1	0.1	0.1	H
Violin Mode	1379.52	1	0.1	0.1	H
Violin Mode	1389.06	1	0.06	0.06	H
Violin Mode	1389.82	1	0.07	0.07	H
Violin Mode	1391.5	1	0.2	0.2	H
Violin Mode	1372.925	1	0.075	0.075	L
Violin Mode	1374.7	1	0.1	0.1	L
Violin Mode	1375.2	1	0.1	0.1	L
Violin Mode	1378.39	1	0.1	0.1	L
Violin Mode	1387.4	1	0.05	0.05	L
Violin Mode	1388.5	1	0.3	0.3	L

1260
1320
1380
1440
1500
WHY NOT LIST INDIVIDUALLY ?

TABLE III. Instrumental lines identified and cleaned before the Einstein@Home analysis. The different columns represent: (I) the source of the line; (II) the central frequency of the instrumental line; (III) the number of harmonics; (IV) Low-Frequency-Side (LFS) of the knockout band; (V) High-Frequency-Side (HFS) of the knockout band; (VI) the interferometer where the instrumental lines were identified. Note that when there are higher harmonics present, the knockout bandwidth remains constant.

3. Signal-frequency ranges and Data Quality

Source	Mixed (Isolated)	Mixed (Left)	All Fake Data	Mixed (Right)	IFO
Power Mains	– –	1258.8146 – 1259.2194	1259.2194 – 1260.8144	1260.8144 – 1261.2196	H,L
Power Mains	– –	1318.8085 – 1319.2255	1319.2255 – 1320.8083	1320.8083 – 1321.2257	H,L
Violin Mode	1372.6530 – 1373.2310	– –	– –	– –	L
Violin Mode	1373.4529 – 1374.0811	– –	– –	– –	H
Violin Mode	1374.1529 – 1375.5312	– –	– –	– –	H,L
Violin Mode	1376.8526 – 1377.4814	– –	– –	– –	H
Violin Mode	1378.1025 – 1379.0816	– –	– –	– –	H,L
Power Mains	– –	1378.8024 – 1379.2316	1379.2316 – 1380.8022	1380.8022 – 1381.2318	H,L
Violin Mode	1387.1516 – 1387.6825	– –	– –	– –	L
Violin Mode	– –	1388.0015 – 1388.4325	1388.4325 – 1388.6014	1388.6014 – 1389.0326	H,L
Violin Mode	1388.8014 – 1389.3826	– –	– –	– –	H,L
Violin Mode	1389.5513 – 1390.1327	– –	– –	– –	H
Violin Mode	1391.1012 – 1391.9329	– –	– –	– –	H,L
Power Mains	– –	1438.7963 – 1439.2377	1439.2377 – 1440.7961	1440.7961 – 1441.2379	H,L
Power Mains	– –	1498.7902 – 1499.2438	1499.2438 – 1499.4901	1499.4901 – 1499.7170	H,L

TABLE IV. Signal-frequency ranges where the results might have contributions from fake data. When the results are entirely due to artificial data, the band is listed in the "All Fake Data" column; bands where the results comprise of contributions from both fake and real data are listed in the other three columns. The "Mixed (Left)" and "Mixed (Right)" columns are populated only when there is a matching "All Fake Data" entry, which highlights the same physical cause for the fake data, i.e. the cleaning. The "Mixed (Isolated)" column lists isolated ranges of mixed data. The list of input data frequencies where the data was substituted with artificial noise are given in table III.

include

THE 3 MIXED COLUMNS ARE CONFUSING. I GET IT, BUT MORE EXPLANATION WOULD BE HELPFUL. FOR EXAMPLE, YOU COULD EXPLAIN WHY THE POWER MAINS CAN HAVE ALL FAKE DATA, BUT NOT THE VIOLIN MODES